Passive Elasticity in a Model of Snake Locomotion

Angelia Wang
under Dr. Xiaolin Wang, Ph.D. and Dr. Silas Alben, Ph.D.
University of Michigan, Ann Arbor, MI

Abstract

Snake locomotory dynamics is an interesting field of study to biologists, physicists, and undergraduate applied mathematicians. In this project, we study a simple model problem of an elastic beam moving on a frictional surface. The beam could model an elastic tail of a snake or a sand-swimming lizard. Previous studies have laid out a great deal of groundwork on the motions of bodies with prescribed shapes, but less work has been done on the motions of elastic bodies. To that end, this project incorporates passive elasticity into the model using a fourth-order partial differential equation system that draws from Euler-Bernoulli beam dynamics with the ultimate goal of exploring how various external and internal forces affect both short-term movements and long-term dynamics of the snake body. This work can be extended to studies in robotics, physics, and fluids.

I. Introduction

Snakes are fundamentally different from other vertebrates because they lack limbs, and their locomotion is similarly distinct from other forms of movement such as swimming, walking, or flying. Unlike the movements of limbed animals, each method of snake locomotion is distinct from the others. Those methods include side-winding, rectilinear movement, concertina motion, and slithering or serpentine movement. Additionally, robots that imitate snake movement have performed exceptionally well in narrow spaces and rough terrain.

We focus on the undulatory motions of snakes on a horizontal plane with fixed axes x and y. The snake is represented as a one-dimensional curved body whose position can be parametrized by arc length (s) and time (t).

The following are variables used in this project:

s = arc length, nondimensionalized
ρ = the snake's mass per unit length, assumed constant
L = length of the snake, often normalized to 1
μ_f = coefficient of forward (tangential) friction
μ_b = coefficient of backward friction
μ_t = coefficient of horizontal (transverse) friction, assumed to be no smaller than μ_f
$\mathbf{X}(s,t) = (x(s,t),\ y(s,t))$ = position of the snake body
$\kappa(s,t)$ = curvature at a given point

There are external forces acting on the snake body: gravity and friction with the horizontal surface. We assume that the friction coefficient in the transverse (horizontal) direction is larger than in the tangential (forward) direction, which is typically true in both robotic models of snakes and biological snakes. Previous studies have found that similar models are remarkably faithful to the mechanics of biological snakes on horizontal planes and have used those models to find optimally efficient snake motions.

Previous work prescribed snake locomotion as a retrograde traveling wave with variable amplitudes. While we take no assumptions about the shape of the snake movement, we retain many of the same metrics. Amplitude, for instance, is measured in the y-direction.

II. Basic Model

The snake body is a curvilinear (planar curve) segment whose position is written as a function of arc length and time.

$$\mathbf{X}(s,t) = (x(s,t),\ y(s,t)).$$

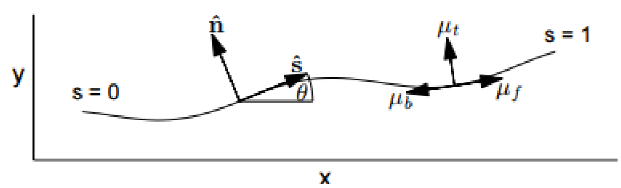

Figure 1: *Schematic of the snake's position on a horizontal plane The arc length s is nondimensionalized and normalized such that $s \in [0,1]$. The coefficients μ_f and μ_b are tangential to the snake body, whereas μ_t is orthogonal. The vectors $\hat{n}$ and $\hat{s}$ are unit vectors normal and tangential to snake movement, respectively. The dimensions x and y are fixed and do not correspond to the direction of movement of the snake.*

Define the tangent angle and the curvature as $\theta(s,t)$ and $\kappa(s,t)$ respectively.

Curvature is a measure of how rounded the snake body is at a particular point. It can be calculated as the partial derivative of tangent angle with respect to arc length.

$$\kappa(s,t) = \frac{\partial}{\partial s}\theta(s,t)$$

$\kappa(s,t)$ is also equivalent to the inverse of the radius R of the circle bordering the snake at arc length s and time t.

At small values of θ, we can approximate κ as follows.

$$\theta \approx \tan\theta = \partial_x y$$
$$\kappa = \partial_s \theta \approx \partial_x \theta \approx \partial_x^2 y$$

Conversely, given $\kappa(s,t)$, we can integrate to find the tangent angle θ and position of the snake body.

$$(1) \quad \theta(s,t) = \theta_0(t) + \int_0^s \kappa(u,t)du$$

$$(2) \quad x(s,t) = x_0(t) + \int_0^s \cos\theta(u,t)du$$

$$(3) \quad y(s,t) = y_0(t) + \int_0^s \sin\theta(u,t)du$$

The coordinates of the tail (x_0, y_0) and the angle of the tail θ_0 can be determined by external forces and torque balances on the snake, but we will omit the calculations here. See X. Wang *et. al* for the appropriate derivations.

The force per unit length on the snake $\mathbf{f}$ can be calculated as the sum of the forces in the transverse, forward, and backward directions. the snake experiences friction with different coeffcients in different directions. The relevant frictional coefficients are μ_f, μ_b, and μ_t for movement in the forward ($\hat{s}$), backward ($-\hat{s}$), and transverse/normal directions ($\hat{n}$), respectively. A negative sign denotes that a frictional force component acts in the opposite direction to motion.

Thus, the total force per unit length due to Coulomb friction with the ground is

$$\mathbf{f}(s,t) = -\rho g \left\{ \mu_t \left(\widehat{\partial_t \mathbf{X}} \cdot \widehat{n} \right) \widehat{n} + \left(\widehat{\partial_t \mathbf{X}} \cdot \widehat{s} \right) \widehat{s} \left[\mu_f \mathbb{1}_{(\widehat{\partial_t \mathbf{X}} \cdot \widehat{s}) > 0} + \mu_b \mathbb{1}_{(\widehat{\partial_t \mathbf{X}} \cdot \widehat{s}) < 0} \right] \right\}$$

Hats indicate normalized vectors, $\mathbb{1}$ is the indicator function, and $\partial_t \mathbf{X} = (\partial_t x(s,t), \partial_t y(s,t))$. The notation $\left(\widehat{\mathbf{V}} \cdot \widehat{d} \right) \widehat{d}$ denotes the resolution of vector V into its component along the $\hat{d}$ direction. We define $\widehat{\partial_t \mathbf{X}} = 0$ when the snake velocity is 0.

III. Passive Elasticity

I. Setup

Suppose the snake is made up of segments, each of infinitessimal length Δs. There is an external frictional force density applied across the length of the snake.

The snake body has certain properties.

E = Young's modulus, a measure of resistance to bending
I = the second moment of area about the beam's cross section????
B = the product EI, a measure of the beam's rigidity

Any fixed segment experiences a series of forces from its neighbors. These forces can be divided into its components in the normal direction and in the tangential direction. We'll call the tangential force **tension**, denoted $T(s,t)\hat{s}$ and the normal force the **shearing force**, denoted $Q(s,t)\hat{n}$.

As a result of these neighboring forces, a segment will also have an internal bending moment, denoted $M(s,t)$, which can be thought of the torque produced by the movement of an adjacent segment, about the axis coming out of the page. It can be calculated as follows.

$$M(s,t) = EI\kappa(s,t) = B\kappa(s,t)$$

II. Torque Balances

Consider an arbitrary but fixed segment of length Δs along the snake body, and assume that the segments on either side of it are bent downwards within the plane. The first breakage point occurs at arc length s and the second occurs at arc length $s + \Delta s$.

If the curvature is relatively small, we can approximate the total shearing force along the center segment as $Q(s + \Delta s, t) \times \Delta s$. For a snake in equilibrium, the sum of all forces on the center segment must sum to zero.

$$M(s+\Delta s,t) - M(s,t) + Q(s+\Delta s,t) \times \Delta s = 0$$

Note that we take the negative of $M(s,t)$ to represent a torque at arc length s that is rotating in the opposite direction than at arc length $s+\Delta s$.

Dividing both sides by Δs and taking the limit as $\Delta s \to 0$ gives

$$\partial_s M + Q = 0$$
$$-\partial_s B\kappa = Q$$

III. Force Balances

By similar reasoning, the sum of forces on a segment of the snake in equilibrium should also sum to zero.

$$T(s+\Delta s)\hat{s} - T(s)\hat{s} + Q(s+\Delta s)\hat{n} - Q(s)\hat{n} + \int_s^{s+\Delta s} f(s',t)ds' = 0$$
$$\partial_s \left(T(s,t)\hat{s}\right) + \partial_s(Q\hat{n}) + f(s,t) = 0$$
$$\partial_s \left(T(s,t)\hat{s}\right) + \partial_s(Q\hat{n}) + f(s,t) = 0$$

And substituting the result of Subsection 1 gives

$$\partial_s \left(T(s,t)\hat{s}\right) - \partial_s(\partial_s(B\kappa)\hat{n}) + f(s,t) = 0$$

In the circumstances of a snake with nonzero acceleration, substitute 0 with $\rho\Delta s \times \partial_{tt}\mathbf{X}$. The final equation is

$$\partial_s \left(T(s,t)\hat{s}\right) - \partial_s(\partial_s(B\kappa)\hat{n}) + f(s,t) = \rho\partial_{tt}\mathbf{X}(s,t)$$

This is a fourth-order differential equation that can be solved with six initial and boundary conditions.

IV. Beam Dynamics

We restrict our discussion to the motion of a flexible beam with one clamped end (leading end) and one free edge (tail end). The length of the beam is assumed to be much larger than any other dimension, so the model is one-dimensional. As previously mentioned, the governing equation describing beam position is

$$\partial_s \left(T(s,t)\hat{s}\right) - B\partial_s(\partial_s(\kappa)\hat{n}) + f(s,t) = \rho\partial_{tt}\mathbf{X}(s,t)$$

where $f(s,t)$ is the external frictional force. Without loss of generality, we use $\mu_f \leq \mu_b$ so that forward friction is at most backward friction.

The leading edge position is prescribed a sinusoidal wave with frequency ω.

$$\mathbf{X}(0,t) = A(cos(\omega t) - 1), \partial_s\mathbf{X}(0,t) = 0$$

Because the trailing edge is a free end, the tension force, shearing force, and bending moment are all zero. The latter implies that curvature is also equal to zero.

$$T(L,t) = \partial_s\kappa(L,t) = \kappa(L,t) = 0$$

We non-dimensionalize the governing equations using beam length L and period of prescribed wave moetion $\tau = 2\pi\omega$. The following dimensionless parameters are obtained.

$$\tilde{B} = \frac{B\tau^2}{\rho L^4},\ \tilde{\mu}_t = \frac{g\mu_t\tau^2}{L},\ \tilde{\mu}_f = \frac{g\mu_f\tau^2}{L},\ \tilde{\mu}_b = \frac{g\mu_b\tau^2}{L},\ \tilde{A} = \frac{A}{L}$$

These give us the following dimensionless equations:

$$\rho\partial_{tt}\mathbf{X}(s,t) = \partial_s\left(T(s,t)\hat{s}\right) - B\partial_s(\partial_s(\kappa)\hat{n}) + f(s,t)$$

$$\mathbf{f}(s,t) = -\rho g\left\{\mu_t\left(\widehat{\partial_t\mathbf{X}}\cdot\widehat{n}\right)\widehat{n} + \left(\widehat{\partial_t\mathbf{X}}\cdot\widehat{s}\right)\widehat{s}\left[\mu_f\mathbb{1}_{(\widehat{\partial_t\mathbf{X}}\cdot\widehat{s})>0} + \mu_b\mathbb{1}_{(\widehat{\partial_t\mathbf{X}}\cdot\widehat{s})<0}\right]\right\}$$

with the boundary conditions

$$\begin{gathered}\mathbf{X}(0,t) = \tilde{A}(cos(t\pi t) - 1)\\ \partial_s\mathbf{X}(0,t) = 0\\ T(1,t) = \partial_s\kappa(1,t) = \kappa(1,t) = 0\end{gathered}$$

This nonlinear fourth order system is solved using Broyden's method, an iterative algorithm that finds roots in differential systems. We note that Broyden's method may not necessarily converge when applied to nonlinear systems such as this one.

Below are some examples of beam movement (over one period) and height of the tail end position (as a function of time).

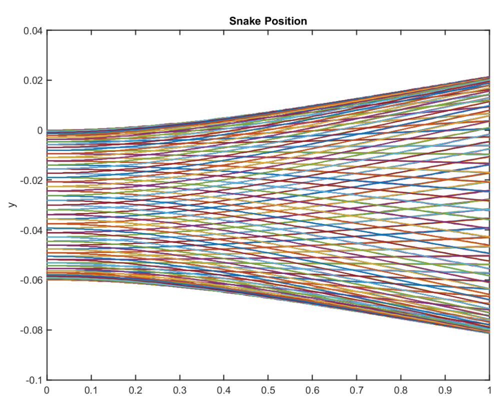

Figure 2: *Beam Position, B = 10*

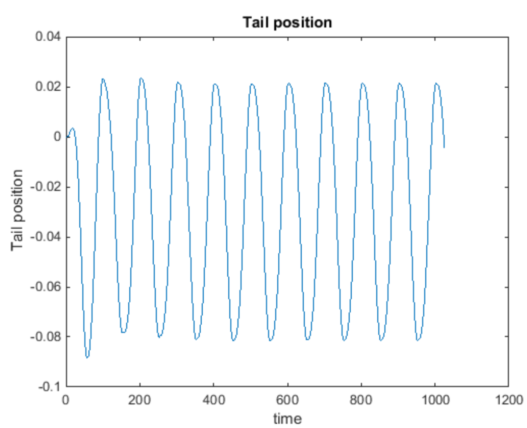

Figure 3: *Tail Position, B = 10*

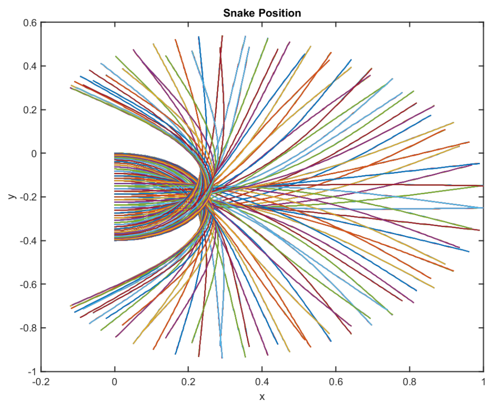

Figure 4: *Beam Position, B = 3*

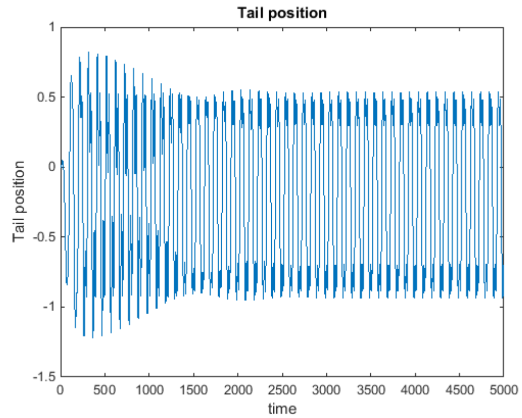

Figure 5: *Tail Position, B = 3*

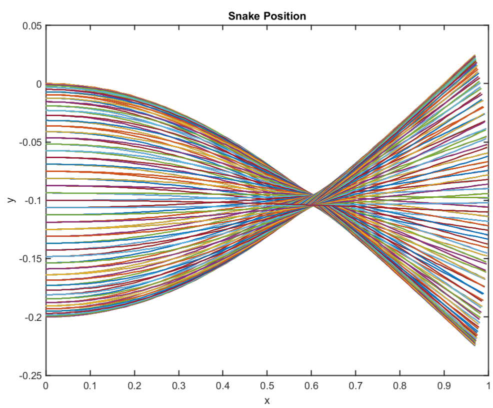

Figure 6: *Beam Position, B = 1*

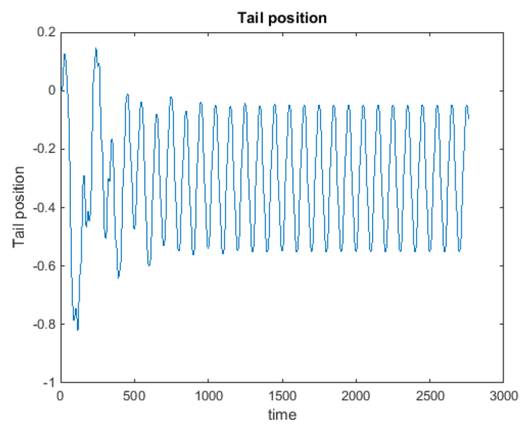

Figure 7: *Tail Position, B = 1*

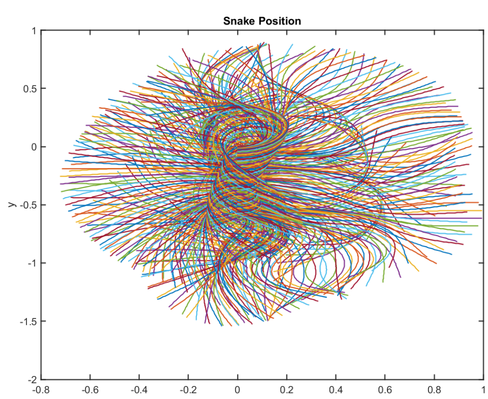

Figure 8: *Beam Position, B = 0.3*

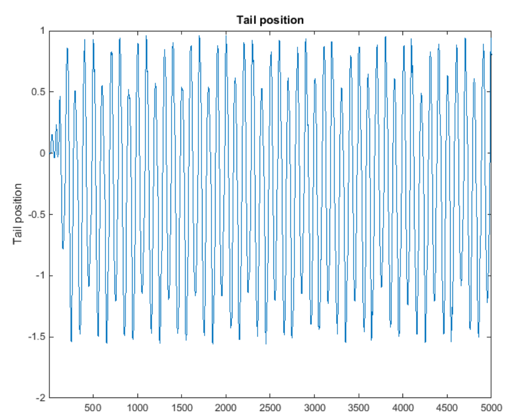

Figure 9: *Tail Position, B = 0.3*

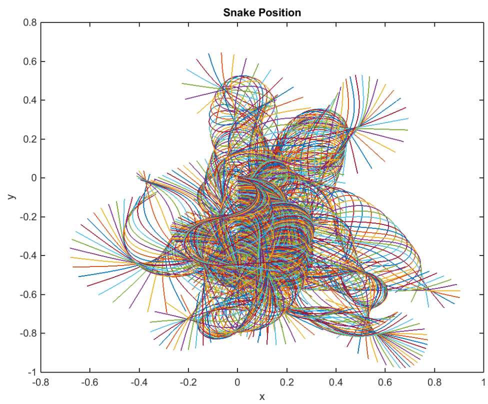

Figure 10: *Beam Position, B = 0.1*

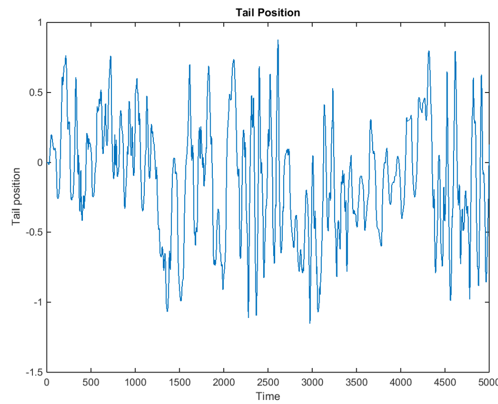

Figure 11: *Tail Position, B = 0.1*

Recall that B is a measure of beam rigidity, so higher values of B correspond to more rigid beams.

Figures 3, 5, 7, 9, and 11 plot the vertical position of the tail end, which allows us to visualize beam movement. Specifically, tail movements that resemble sinusoidal waves suggest that those conditions lead to periodic beam movement. We notice that tail end positions for larger values of B appear to be sinusoidal whereas smaller values of B produce more chaotic movement.

V. Order of Convergence

Our code is deterministic, but that does not guarantee convergence. Convergence studies are used to investigate whether our results converge to fixed values as we increase the level of precision, and if so, how quickly. Our project uses one main ways of increasing precision: increasing the number of gridpoints. That is, we approximate beam position using n evenly spaced gridpoints along its length.

The theory of convergence is as follows.

Suppose that we are trying to approximate a value x, which in our case is unknown. We'll use a step size of size h and gradually decrease it.

We assume that the size of our error is proportional to some power p of the step size. This gives us the following series of equations.

$$x = x_h + Ch^p$$
$$x = x_{\frac{h}{2}} + C\left(\frac{h}{2}\right)^p$$
$$\dots$$

Taking the difference between consecutive equations gives

$$x_h - x_{\frac{h}{2}} = Ch^p - C\left(\frac{h}{2}\right)^p$$
$$x_{\frac{h}{2}} - x_{\frac{h}{4}} = C\left(\frac{h}{2}\right)^p - C\left(\frac{h}{4}\right)^p$$

And the ratio of $Ch^p - C\left(\frac{h}{2}\right)^p$ to $C\left(\frac{h}{2}\right)^p - C\left(\frac{h}{4}\right)^p$ is

$$\left(Ch^p - C\left(\frac{h}{2}\right)^p\right) / \left(C\left(\frac{h}{2}\right)^p - C\left(\frac{h}{4}\right)^p\right) = 2^p$$

The value of p is our order of convergence. Using this procedure with our project finds that both $\mathbf{X}(s,t)$ and $\kappa(s,t)$ converge in second order with respect to gridpoint size. Further studies may uncover why.

VI. Periodicity

As mentioned before, beam motion looks to be periodic under some conditions and chaotic under others. Part of our project attempted to learn more about which conditions led to periodic movement. To that end, I ran simulations for each set of parameters until either the program terminated (suggesting 1-periodic behavior) or reached 500 periods without termination.

$$B = \{0.3, 1, 3, 10\}$$

$$\mu_t = \mu_f = \mu_b = \{0, 0.1, 0.3, 1\}$$
$$A = \{0.03, 0.1, 0.2, 0.3\}$$

To include a condition for termination, the following lines of code were added after each time iteration. $k1$ is the current iteration. ZetaVals is an $n \times k1$ complex matrix that stores values of the beam's position, and DtZetaVals is an $n \times k1$ complex matrix that stores values of the beam's velocity.

```
%%%%%%%%%%%%%%%%%%%%%%%%%%%%%%%%
if k1 > 100
cond1 = (norm(ZetaVals(:, k1) - ZetaVals(:, k1-100))/norm(ZetaVals(:, k1-100)) < 1e-4);
cond2 = (norm(DtZetaVals(:, k1) - DtZetaVals(:, k1-100))/norm(DtZetaVals(:, k1-100)) < 1e-4);
end
if k1 > 100 && cond1 && cond2;
    break
end
```

The if statement checks whether both the beam position and beam velocity is sufficiently close to their corresponding values one period ago, and if so, breaks the loop. Note that this condition only checks whether conditions are sufficient to give 1-periodic motion, and additional tests are needed to check for period doubling or quadrupling.

Using this code, we found that larger values of B tended to correspond to nonperiodic motion, particularly for higher values of A. In contrast, smaller values of B tended to give rise to periodic motion, especially for smaller values of A. In general, increasing the amplitude while holding all other parameters constant caused beam motion to transition from periodic to nonperiodic. Full (preliminary) results are below. Numbers indicate the iteration at which code terminated.

	mu = 0				mu = 0.1				mu = 0.3				mu = 1			
	A = 0.03	A = 0.1	A = 0.2	A = 0.3	A = 0.03	A = 0.1	A = 0.2	A = 0.3	A = 0.03	A = 0.1	A = 0.2	A = 0.3	A = 0.03	A = 0.1	A = 0.2	A = 0.3
B = 0.3	no	no	no	no	2635	6483	no	no	994	4036	5844	no	1858	1127	2088	no
B = 1	no	no	no	no	2521	7273	11910	no	1084	2575	5230	7867	1044	1083	1864	2760
B = 3	no	9010	5758	5359	no	8223	5375	5360	14595	8066	5258	5257	830	6562	4805	4407
B = 10	no	no	no	no	no	no	no	no	6258	no	no	no	1025	4010	no	no

We studied one particular bifurcation in detail. For the values $B = 0.3$ and $\mu_t = \mu_f = \mu_b = 1$, motion transitions from periodic to chaotic somewhere between $A = 0.2$ and $A = 0.3$.

One way to visualize long-term behavior is to look at the position of the trailing edge over time. Moreover, instead of plotting the tail end position at every time iteration, we'll plot one data point per period. If a set of parameters leads to long-term periodic behavior, these plots will show convergence to some horizontal asymptote.

The following are the results of gradually increasing the value of A (continued on next page).

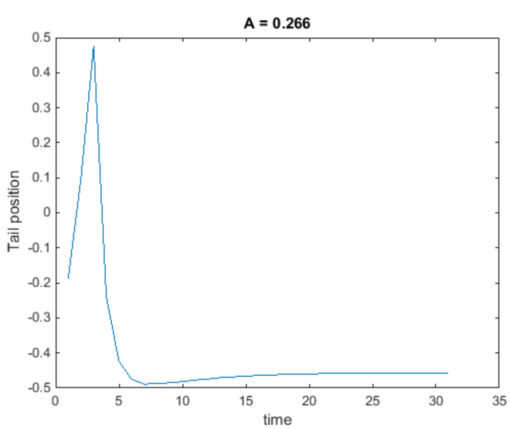

Figure 12: $A = 0.266$

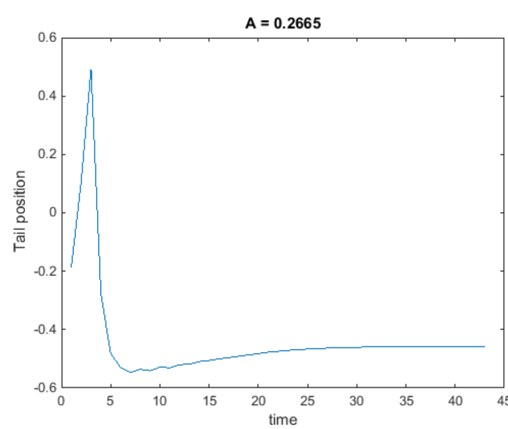

Figure 13: $A = 0.2665$

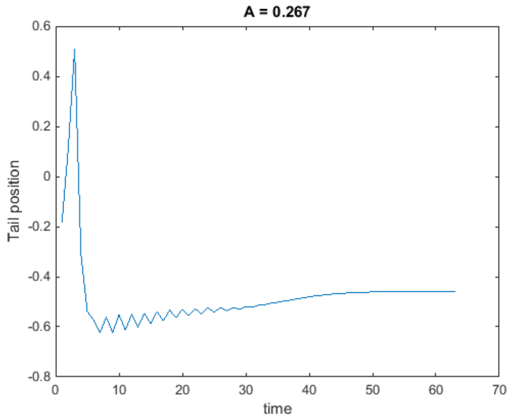

Figure 14: A = *0.267*

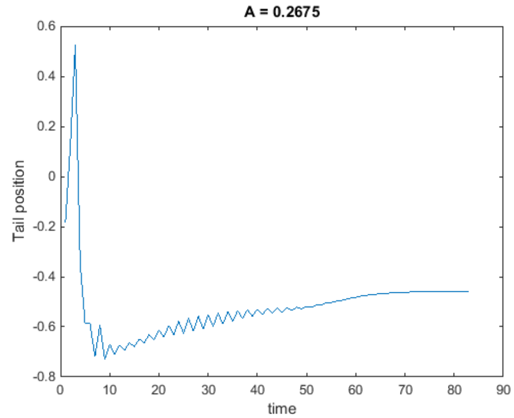

Figure 15: A = *0.2675*

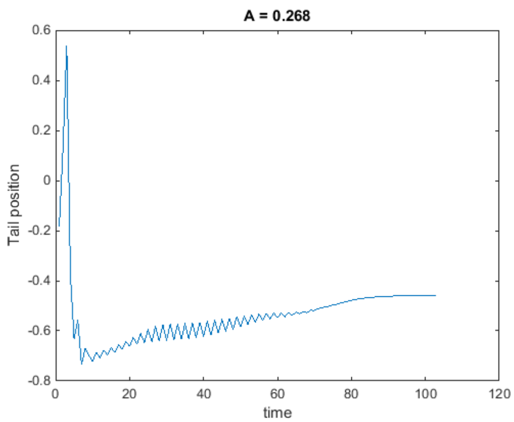

Figure 16: A = *0.268*

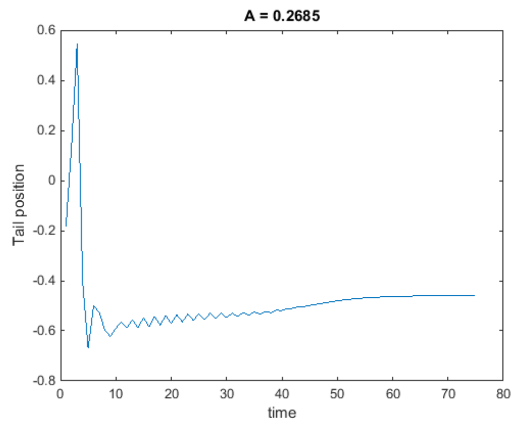

Figure 17: A = *0.2685*

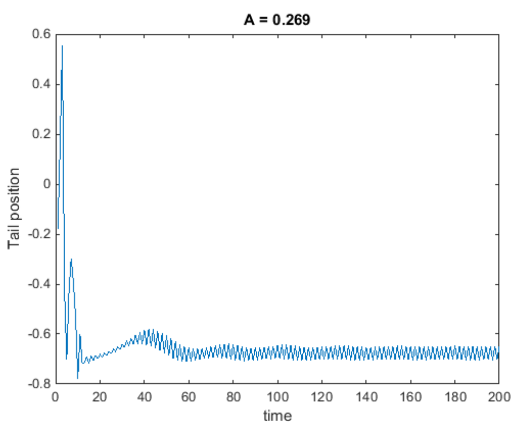

Figure 18: A = *0.269*

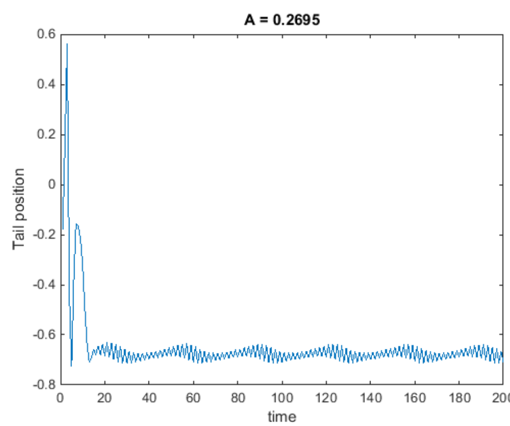

Figure 19: A = *0.2695, showing potentially long-term periodic motion*

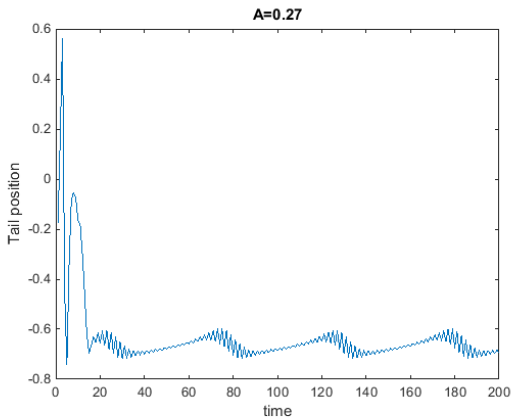

Figure 20: *A = 0.27*

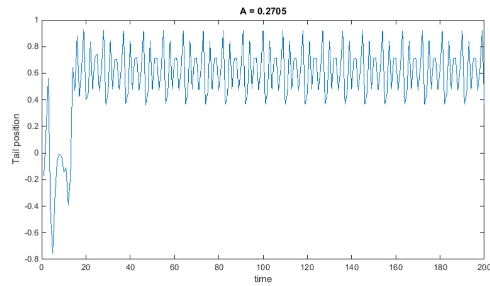

Figure 21: *A = 0.2705*

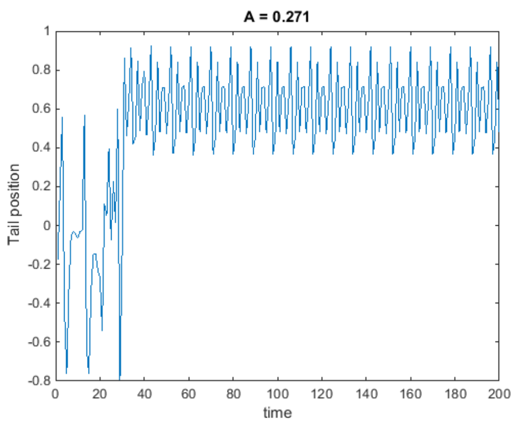

Figure 22: *A = 0.271 shows 9-periodic motion*

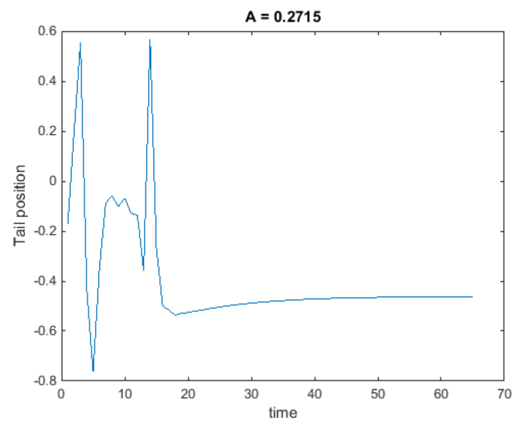

Figure 23: *A = 0.2715 goes back to 1-periodic*

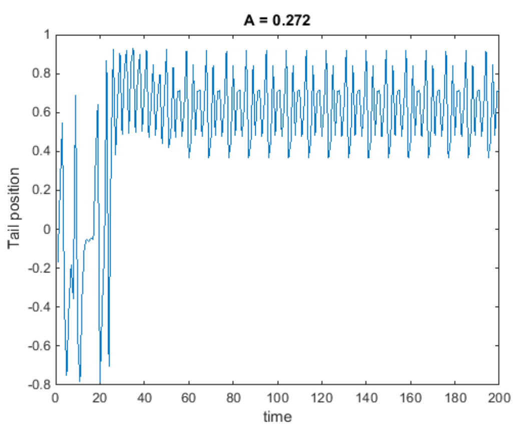

Figure 24: *A = 0.272*

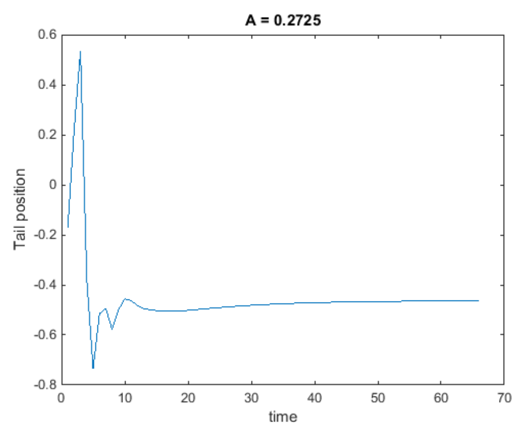

Figure 25: *A = 0.2725*

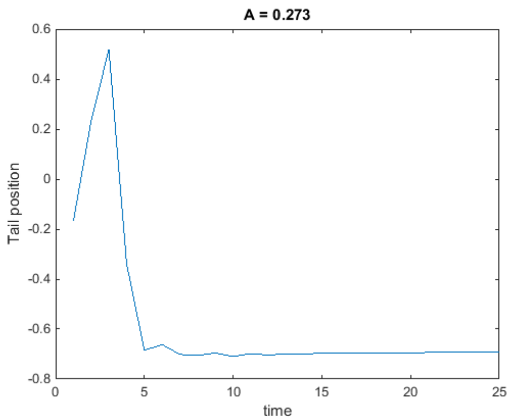

Figure 26: A = *0.273*

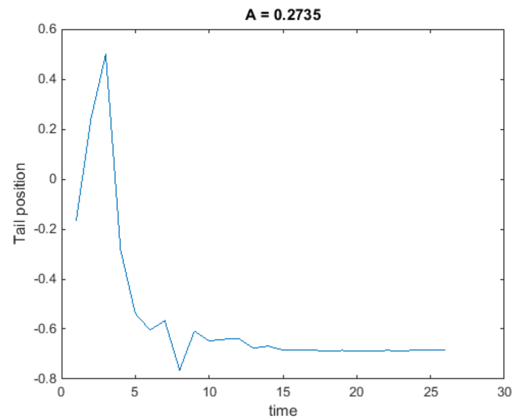

Figure 27: A = *0.2735*

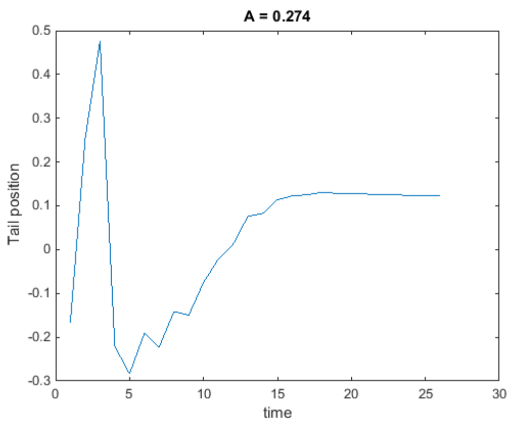

Figure 28: A = *0.274*

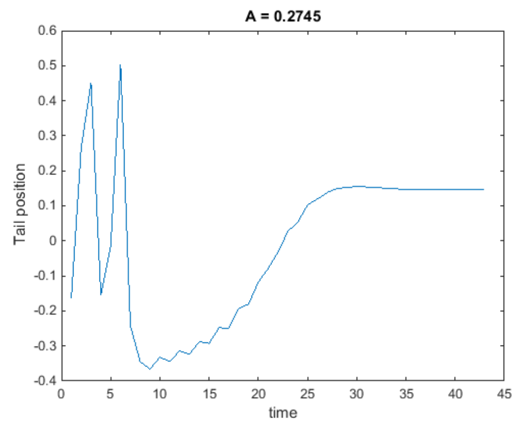

Figure 29: A = *0.2745*

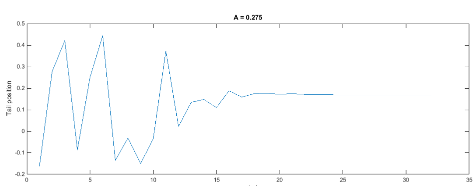

Figure 30: A = *0.275*

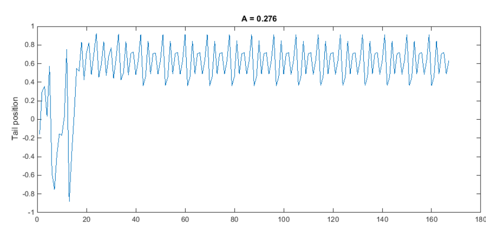

Figure 31: A = *0.276*

All further values of A show similar 9-periodic behavior. Further studies may uncover more about this phenomenon.

VII. Future Directions

My most immediate goal is to explore potential bifurcations in more detail through carrying out more detailed periodic tests. Specifically, find out at what parameters beam motion becomes two- or four-periodic, and investigate how the motion changes as we vary each parameter. In conjunction with this, we'd also like to find out more about transitory periods and exploring why we might be seeing nine-periodic behavior.

Finally, further studies may also uncover why we see second order convergence of our values.

VIII. Acknowledgements

This project would not have been possible without generous funding from the NSF (Grant 0955463).

Additional infinite gratitude goes to Dr. Xiaolin Wang, Ph.D. and Dr. Silas Alben, Ph.D. for countless hours of mathematical guidance and MATLAB help. Special thanks also to Carrie Berger and the University of Michigan Mathematics Department staff for their huge efforts in coordinating and planning logistics... running an REU can't be easy. Finally, I extend my sincere thanks to the university community – specifically, the UM Ballroom Dance Team and the wonderful permanent residents of the REU room – for a summer's worth of love and moral support. You guys are the best.

References

[1] X. Wang, M. Osborne, S. Alben. Optimizing snake locomotion on an inclined plane. Physical Review E **00**, 002700 (2014).

[2] C. Wiggins, R. Goldstein. Flexive and Propulsive Dynamics of Elastica at Low Reynolds Number. Physical Review Letters **00**, 3879 (1998).

[3] "Euler-Bernoulli beam theory." Wikipedia [Online]. Accessed 2015.

[4] "Broyden's method." Wikipedia [Online]. Accessed 2015.